Ultrafast Excited-State Energy Migration Dynamics in an Efficient Light-Harvesting Antenna Polymer Based on Ru(II) and Os(II) Polypyridyl Complexes

Cavan N. Fleming, Kimberly A. Maxwell, Joseph M. DeSimone, Thomas J. Meyer,† and John M. Papanikolas*

Contribution from the Department of Chemistry, Venable and Kenan Laboratories, The University of North Carolina at Chapel Hill, Chapel Hill, North Carolina 27599-3290

Received May 29, 2001

Abstract: A detailed study of the excited state energy migration dynamics that take place within an assembly of Ru(II) and Os(II) polypyridyl complexes linked together through a polymer backbone is presented. The energy migration process is initiated by the photoexcitation of the metal-to-ligand charge transfer (MLCT) transition in one of the Ru(II) complexes and terminated by energy transfer to a lower energy Os(II) trap. Energy transfer sensitization of Os(II) can occur in a single step if the excited state is formed adjacent to a trap, or after a series of hops between isoenergetic rutheniums prior to reaching a trap. The dynamics of the energy transfer process are followed by monitoring the growth of Os(II)* luminescence at 780 nm. The kinetics of the growth are complex and can be fit by a sum of two exponentials. This kinetic complexity arises both from the presence of a distribution of donor−acceptor distances and the variety of time scales by which Os(II)* can be formed. We have augmented the time-resolved experiments with Monte Carlo simulations, which provide insight into the polymer array's structure and at the same time form the basis of a molecular-level description of the energy migration dynamics. The simulations indicate that the most probable Ru*→Os energy transfer time is ∼400 ps while the time scale for Ru*→Ru hopping is approximately 1−4 ns. The time scale for Ru*→Ru hopping relative to its natural lifetime (1000 ns) suggests that this polymer system could be extended to considerably longer dimensions without an appreciable loss in its overall efficiency.

I. Introduction

One strategy for designing functional nanoscale materials is to organize molecular constituents into assemblies that perform complex functions.[1−12] A critical factor in the development of such materials is the ability to control the spatial arrangement of the molecular components, especially if intermolecular energy- and charge-transfer processes are at the core of the material's function. Spatial organization can be achieved through the design of covalently bonded supramolecules in which molecular subunits are linked together so that their relative geometries (i.e. separations and orientations) are well defined.[13−19] Structures of this kind are demanding to synthesize, but offer the greatest amount of control over structural parameters. An alternative method utilizes disordered supports to organize the necessary components.[20−38] Derivatized polymers are attractive for the positioning of molecular constituents because they offer

† Present address: Los Alamos National Laboratory MS A127, Los Alamos, NM 87545.

(1) Alivisatos, A. P.; Barbara, P. F.; Castleman, A. W.; Chang, J.; Dixon, D. A.; Klein, M. L.; McLendon, G. L.; Miller, J. S.; Ratner, M. A.; Rossky, P. J.; Stupp, S. I.; Thompson, M. E. *Adv. Mater.* **1998**, *10* (16), 1297−1336.

(2) Balzani, V.; Gomez-Lopez, M.; Stoddart, J. F. *Acc. Chem. Res.* **1998**, *31*, 405−414.

(3) Balzani, V.; Juris, A.; Venturi, M.; Campagna, S.; Serroni, S. *Chem. Rev.* **1996**, *96*, 759−833.

(4) Collier, C. P.; Mattersteig, G.; Wong, E. W.; Luo, Y.; Beverly, K.; Sampaio, J.; Raymo, F. M.; Stoddart, J. F.; Heath, J. R. *Science* **2000**, *289* (5482), 1172−1175.

(5) Heath, J. R. *Acc. Chem. Res.* **1999**, *32* (5), 388.

(6) Piotrowiak, P. *Chem. Soc. Rev.* **1999**, *28*, 143−150.

(7) Fabbrizzi, L.; Licchelli, M.; Pallavicini, P. *Acc. Chem. Res.* **1999**, *32*, 846−853.

(8) Ward, M. D. *Chem. Soc. Rev.* **1997**, *26*, 364−375.

(9) Benniston, A. C. *Chem. Soc. Rev.* **1996**, 427−435.

(10) Reimers, J. R.; Lu, T. X.; Crossley, M. J.; Hush, N. S. *Nanotechnology* **1996**, *7*, 424−429.

(11) Krische, M. J.; Lehn, J. M. Struct. Bonding **2000**, *96*, pp 3−29.

(12) Ziener, U.; Breuning, E.; Lehn, J. M.; Wegelius, E.; Rissanen, K.; Baum, G.; Fenske, D.; Vaughan, G. *Chem. Eur. J.* **2000**, *6* (22), 4132−4139.

(13) Kleverlaan, C. J.; Indelli, M. T.; Bignozzi, C. A.; Pavanin, L.; Scandola, F.; Hasselman, G. M.; Meyer, G. J. *J. Am. Chem. Soc.* **2000**, *122* (12), 2840−2849.

(14) Bignozzi, C. A.; Argazzi, R.; Kleverlaan, C. J. *Chem. Soc. Rev.* **2000**, *29* (2), 87−96.

(15) Bignozzi C. A.; Schoonover, J. R.; Scandola, F. *Prog. Inorg. Chem.* **1997**, *44*, 1−95.

(16) Gust, D.; Moore, T. A.; Moore, A. L. *J. Photochem. Photobiol., B* **2000**, *58* (2−3), 63−71.

(17) Gust, D.; Moore, T. A.; Moore, A. L. *Acc. Chem. Res.* **2001**, *34* (1), 40−48.

(18) Hissler, M.; Mcgarrah, J. E.; Connick, W. B.; Geiger, D. K.; Cummings, S. D.; Eisenberg, R. *Coord. Chem. Rev.* **2000**, *208*, 115−137.

(19) Slate, C. A.; Striplin, D. R.; Moss, J. A.; Chen, P.; Erickson, B. W.; Meyer, T. J. *J. Am. Chem. Soc.* **1998**, *120*, 4885−4886.

(20) Mallouk, T. E.; Gavin, J. A. *Acc. Chem. Res.* **1998**, *31*, 209−217.

(21) Kaschak, D. M.; Lean, J. T.; Waraksa, C. C.; Saupe, G. B.; Usami, H.; Mallouk, T. E. *J. Am. Chem. Soc.* **1999**, *121*, 3435−3445.

(22) Kaschak, D. M.; Johnson, S. A.; Waraksa, C. C.; Pogue, J.; Mallouk, T. E. *Coord. Chem. Rev.* **1999**, *186*, 403−416.

(23) Kincaid, J. R. *Chem. Eur. J.* **2000**, *6* (22), 4055−4061.

(24) Wu, A.; Yoo, D.; Lee, J. K.; Rubner, M. F. *J. Am. Chem. Soc.* **1999**, *121* (20), 4883−4891.

(25) Mattoussi, H.; Rubner, M. F.; Zhou, F.; Kumar, J.; Tripathy, S. K.; Chiang, L. Y. *Appl. Phys. Lett.* **2000**, *77* (10), 1540−1542.

(26) Baur, J. W.; Rubner, M. F.; Reynolds, J. R.; Kim, S. *Langmuir* **1999**, *15* (19), 6460−6469.

(27) Lee, J. K.; Yoo, D.; Rubner, M. F. *Chem. Mater.* **1997**, *9* (8), 1710.

10.1021/ja016304i CCC: $20.00
Published on Web 10/02/2001

flexibility and simplicity in the design of multicomponent assemblies. The Meyer group has explored this approach in their work on derivatized polystyrene,[39−46] and the controlled positioning of chromophores and other components along a polymer backbone has been demonstrated by other groups as well.[47−59] In this paper we describe ultrafast spectroscopic experiments that are aimed at characterizing the light-harvesting function of a polymer derivatized with Ru(II) and Os(II) chromophores.

The functional capabilities of light-harvesting systems can be quantified on the basis of the efficiency with which they conduct excited-state energy. For efficient conduction to occur, the time scale for energy transfer must be fast compared to the lifetime of the excited state. For example, if the time scale for an excited state to hop to an adjacent site is 10 times faster than its lifetime, energy transfer will occur with 90% efficiency. Thus efficient energy migration is best achieved by combining fast energy transfer between monomer units with long-lived excited states.

A number of attempts have been made to mimic the energy transfer capabilities of biological photosynthetic systems. Early efforts focused on methacrylate polymers functionalized with naphthalene- and anthracene-based chromophores.[60−62] Following photoexcitation, the naphthalene excited state migrates along the polymer backbone until it is quenched by energy transfer to an anthracene trap that exists in low concentrations (∼1%). A wide range of efficiencies has been reported for different systems; however, in general the efficiencies are much less than unity, ranging from 30 to 80%. Fox and co-workers[63−66] investigated a series of diblock and triblock copolymer systems that couple energy migration with electron transfer. In these systems, the rate of energy migration ($\tau \sim 300$ ps) is comparable to the lifetime of the photoexcited donor ($\tau \sim 4$ ns).

Efficient energy conduction has also been observed in porphyrin arrays, and a great deal has been learned about the energy transfer dynamics in these multicentered systems.[67−73] In the case of a Zn/free-base porphyrin dimer, energy transfer to the free base subunit occurs with an efficiency of greater than 95%. When the system is extended to a trimer with two isoenergetic Zn porphyrin donors, the energy hopping between donors occurs with a time constant of ≈50 ps, or 40 times faster than the natural lifetime of the monomer. One consequence of the intrinsically short excited-state lifetime is that energy hopping competes with the decay of the excited state, limiting the energy transfer efficiency. This effect is magnified when there are multiple energy transfer steps. The reported efficiency[73] for donor and acceptor separated by three isoenergetic Zn porphyrins is 76% and calculations indicate that this drops to 13% when the array is extended to 20 monomer units.[71]

In this paper we describe an ultrafast spectroscopic investigation of the photoinduced energy migration dynamics that take place within a supramolecular assembly consisting of 20 Ru(II) and/or Os(II) polypyridyl coordination complexes linked together through a polystyrene backbone (Figure 1). Our experiments are performed on a solution of polymer chains dissolved in acetonitrile, and thus probe the dynamics that occur within individual assemblies. Energy migration is initiated by photoexcitation of one of the Ru(II) complexes and terminated upon energy transfer to a lower energy Os(II) trap. We find that when there is an average of three Os complexes per

(28) Shortreed, M. R.; Swallen, S. F.; Shi, Z.; Tan, W.; Xu, Z.; Devadoss, C.; Moore, J. S.; Kopelman, R. *J. Phys. Chem. B* **1997**, *101*, 6318.
(29) Devadoss, C.; Bharathi, P.; Moore, J. S. *J. Am. Chem. Soc.* **1996**, *118*, 9635.
(30) Balzani, V.; Campagna, S.; Denti, G.; Juris, A.; Serroni, S.; Venturi, M. *Acc. Chem. Res.* **1998**, *31*, 26−34.
(31) Jiang, D.; Aida, T. *J. Am. Chem. Soc.* **1998**, *120*, 10895.
(32) Adronov, A.; Gilat, S. L.; Fréchet, J. M. J.; Ohta, K.; Neuwahl, F. V. R.; Fleming, G. R. *J. Am. Chem. Soc.* **2000**, *122* (6), 1175−1185.
(33) Neuwahl, F. V. R.; Righini, R.; Adronov, A.; Malenfant, P. R. L.; Fréchet, J. M. J. *J. Phys. Chem. B* **2001**, *105*, 1307.
(34) Vögtle, F.; Plevoets, M.; Nieger, M.; Azzellini, G. C.; Credi, A.; Cola, L. D.; Marchis, V. D.; Venturi, M.; Balzani, V. *J. Am. Chem. Soc.* **1999**, *121*, 6290−6298.
(35) Newkome, G. R.; He, E.; Moorefield, C. N. *Chem. Rev.* **1999**, *99*, 1689−1746.
(36) Stewart, G. M.; Fox, M. A. *Chem. Mater.* **1998**, *10*, 860.
(37) Storrier, G. D.; Takada, K.; Abruña, H. D. *Langmuir* **1999**, *15*, 872−884.
(38) Yeow, E. K. L.; Ghiggino, K. P.; Reek, J. N. H.; Crossley, M. J.; Bosman, A. W.; Schenning, A. P. H. J.; Meijer, E. W. *J. Phys. Chem. B* **2000**, *104* (12), 2596−2606.
(39) Worl, L. A.; Jones, W. E.; Strouse, G. F.; Younathan, J. N.; Danielson, E.; Maxwell, K. A.; Sykora, M.; Meyer, T. J. *Inorg. Chem.* **1999**, *38* (11), 2705−2708.
(40) Friesen, D. A.; Kajita, T.; Danielson, E.; Meyer, T. J. *Inorg. Chem.* **1998**, *37* (11), 2756−2762.
(41) Maxwell, K. A.; Dupray, L. M.; Meyer, T. J. *Polym. Prepr. (Am. Chem. Soc., Div. Polym. Chem.)* **1997**, *38*, 329−330.
(42) Dupray, L. M.; Meyer, T. J. *Inorg. Chem.* **1996**, *35* (21), 6299−6307.
(43) Jones, W. E.; Baxter, S. M.; Strouse, G. F.; Meyer, T. J. *J. Am. Chem. Soc.* **1993**, *115* (16), 7363−7373.
(44) Dupray, L. M.; Devenney, M.; Striplin, D. R.; Meyer, T. J. *J. Am. Chem. Soc.* **1997**, *119* (42), 10243−10244.
(45) Peters, M. A.; Belu, A. M.; Linton, R. W.; Dupray, L. M.; Meyer, T. J.; DeSimone, J. M. *J. Am. Chem. Soc.* **1995**, *117* (12), 3380−3388.
(46) Sykora, M.; Maxwell, K. A.; DeSimone, J. M.; Meyer, T. J. *Proc. Natl. Acad. Sci. U.S.A.* **2000**, *97* (14), 7687−7691.
(47) Wong, K. T.; Lehn, J. M.; Peng, S. M.; Lee, G. H. *Chem. Commun.* **2000**, *22*, 2259−2260.
(48) Galoppini, E.; Fox, M. A. *J. Am. Chem. Soc.* **1996**, *118* (9), 2299−2300.
(49) Clements, J. H.; Webber, S. E. *J. Phys. Chem. B* **1999**, *103*, 9366.
(50) Clements, J. H.; Webber, S. E. *J. Phys. Chem. A* **1999**, *103*, 2513−2523.
(51) Schillén, K.; Yekta, A.; Ni, S.; Farinha, J. P. S.; Winnik, M. A. *J. Phys. Chem. B* **1999**, *103*, 9090−9103.
(52) Rharbi, Y.; Yekta, A.; Winnik, M. A.; DeVoe, R. J.; Barrera, D. *Macromolecules* **1999**, *32*, 3241−3248.
(53) Walters, K. A.; Trouillet, L.; Guillerez, S.; Schanze, K. S. *Inorg. Chem.* **2000**, *39* (24), 5496−5509.
(54) Walters, K. A.; Ley, K. D.; Schanze, K. S. *Langmuir* **1999**, *15* (17), 5676−5680.
(55) Mcquade, D. T.; Pullen, A. E.; Swager, T. M. *Chem. Rev.* **2000**, *100* (7), 2537−2574.
(56) Swager, T. M. *Acc. Chem. Res.* **1998**, *31* (5), 201−207.
(57) Chen, L. X.; Jäger, W. J. H.; Gosztola, D. J.; Niemczyk, M. P.; Wasielewski, M. R. *J. Phys. Chem. B* **2000**, *104* (9), 1950−1960.
(58) Chen, L. X.; Jäger, W. J. H.; Niemczyk, M. P.; Wasielewski, M. R. *J. Phys. Chem. A* **1999**, *103* (22), 4341−4351.
(59) Wolcan, E.; Ferraudi, G. *J. Phys. Chem. A* **2000**, *104* (41), 9281−9286.
(60) Webber, S. E. *Chem. Rev.* **1990**, *90*, 1469−1482.
(61) Holden, D. A.; Guillet, J. E. *Macromolecules* **1980**, *13*, 289.
(62) Ng, D.; Guillet, J. E. *Macromolecules* **1982**, *15*, 724.
(63) Fox, M. A. *Acc. Chem. Res.* **1999**, *32*, 201−207.
(64) Watkins, D. M.; Fox, M. A. *J. Am. Chem. Soc.* **1996**, *118*, 4344−4353.
(65) Whitesell, J. K.; Chang, H. K.; Fox, M. A.; Galoppini, E.; Watkins, D. M.; Fox, H.; Hong, B. *Pure Appl. Chem.* **1996**, *68*, 1469−1774.
(66) Fox, M. A. *Macromol. Symp.* **1996**, *101*, 219−226.
(67) Li, J.; Lindsey, J. S. *J. Org. Chem.* **1999**, *64* (25), 9101−9108.
(68) Li, J.; Ambroise, A.; Yang, S. I.; Diers, J. R.; Seth, J.; Wack, C. R.; Bocian, D. F.; Holten, D.; Lindsey, J. S. *J. Am. Chem. Soc.* **1999**, *121* (38), 8927−8940.
(69) Kuciauskas, D.; Liddell, P. A.; Lin, S.; Johnson, T. E.; Weghorn, S. J.; Lindsey, J. S.; Moore, A. L.; Moore, T. A.; Gust, D. *J. Am. Chem. Soc.* **1999**, *121* (37), 8604−8614.
(70) Li, F.; Yang, S. I.; Ciringh, Y.; Seth, J.; Martin, C. H.; Singh, D. L.; Kim, D.; Birge, R. R.; Bocian, D. F.; Holten, D.; Lindsey, J. S. *J. Am. Chem. Soc.* **1998**, *120* (39), 10001−10017.
(71) Van Patten, P. G.; Shreve, A. P.; Lindsey, J. S.; Donohoe, R. J. *J. Phys. Chem. B* **1998**, *102*, 4209.
(72) Cho, H. S.; Song, N. W.; Kim, Y. H.; Jeoung, S. C.; Hahn, S.; Kim, D.; Kim, S. K.; Yoshida, N.; Osuka, A. *J. Phys. Chem. A* **2000**, *104* (15), 3287−3298.
(73) Wagner, R. W.; Lindsey, J. S. *J. Am. Chem. Soc.* **1994**, *116*, 9759.

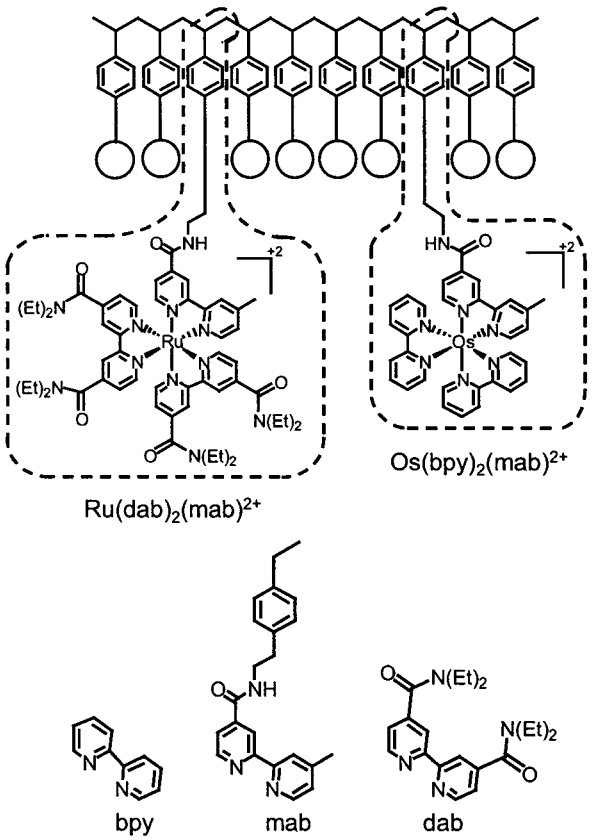

Figure 1. Schematic diagram depicting the structure of the polymeric assembly. Ru(II) and Os(II) complexes are covalently linked to a polystyrene backbone. Open circles in the diagram represent other transition metal complexes that are not shown for clarity. The structures of the two monomer complexes, $Ru(dab)_2(mab)^{2+}$ and $Os(bpy)_2(mab)^{2+}$, are identified by the dashed lines. Our experiments were performed on polymer chains dissolved in CH_3CN. At the bottom of the figure are the chemical structures of the three ligands (bpy, mab, and dab) referred to in the text.

chain the sensitization efficiency of the Os sites by photoexcited Ru complexes is near unity (≈95%). Although this efficiency is an indicator of its light-harvesting potential, its value depends on the degree of Os loading, and thus does not provide a window through which to view the microscopic dynamics.

To gain a better understanding of the *intrinsic* properties of the energy migration process we have augmented our time-resolved experiments with Monte Carlo simulations. These provide insight into the polymer array's structure and at the same time form the basis of a molecular-level description of the energy migration dynamics. Our simulations suggest that the Ru*→Ru energy transfer times are in the range between 1 and 4 ns, or about 250−1000 times faster than the natural lifetime of the Ru excited state (1000 ns). This implies a single-step energy transfer efficiency of 99.6 to 99.9%. The fast excited state hopping relative to the Ru excited state lifetime suggests that an excited state could make a large number of hops, and thus transport excited state energy over long distances with relatively high efficiency.

II. Experimental Section

A. Synthesis and Materials. The primary focus of our spectroscopic experiments is on the polymeric system with mixed Ru(II)/Os(II) loading, $PS\text{-}Ru_{17}Os_3$. The synthesis of this system is described fully elsewhere[40,74] and so only a brief description is given here. The synthesis of the polystyrene backbone, $PS\text{-}CH_2CH_2NH_2$, is accomplished via a living anionic polymerization of a vinyl monomer with a protected amine group. The living anionic method offers the advantage of decreased molecular weight polydispersity compared to free radical techniques (PDI = 1.08). In the present work, the polymerization was terminated at 20 repeat units. The loading of the polystyrene backbone is accomplished by amide coupling of the deprotected amine with carboxylic acid derivatized Ru and Os complexes. In the case of the mixed-loaded polymers, the minority species is loaded first by reacting the deprotected polymer with 3 equiv of Os(II) complex per polymer chain. The remaining sites are then loaded with Ru(II) complexes via reaction with an excess of the acid functionalized Ru(II) compound. The degree of metal site vacancies (i.e. binding sites with no attached complex) was assessed by using ^{1}H NMR.[41] The 17:3 Ru/Os loading ratio was confirmed by ^{1}H NMR and UV−vis absorption measurements. Spectroscopic experiments are performed on polymer chains dissolved in room temperature acetonitrile.

B. Steady-State Methods. UV−visible spectra were recorded on a diode array spectrometer with 2 nm resolution. The spectroscopic grade acetonitrile used in the photophysical measurements was either used as received or distilled over CaH_2. Steady state emission spectra were recorded on a photon counting spectrofluorimeter and were corrected for the instrument response. Optically dilute samples (less than 0.12 OD at the excitation wavelength) were Argon sparged for 40 min prior to use. Emission quantum yields were determined by relative actinometry.[75] The procedure involves the measurement of the integrated emission profile (I) and absorbance (A) of an unknown sample and a reference compound. The quantum yield of the sample (Φ) is then determined by using

$$\Phi = \Phi_R\left(\frac{I}{I_R}\right)\left(\frac{n}{n_R}\right)^2\left(\frac{A_R}{A}\right) \quad (1)$$

where n is the refractive index of the solvent, and Φ_R, A_R, and n_R all refer to the reference compound. The reference used in this work was either $[Ru(bpy)_3](PF_6)_2$, for which $\Phi_{em} = 0.062$,[76] or $[Os(bpy)_3](PF_6)_2$, for which $\Phi_{em} = 0.005$,[77] in acetonitrile at 298 K.

C. Time-Resolved Emission Methods. Time-resolved measurements were conducted by time-correlated single photon counting (TCSPC). The apparatus consists of a mode-locked Nd:YAG laser (Coherent Antares) whose frequency tripled output is used to synchronously pump a single jet dye laser with Stilbene 3. The dye laser output at 430 nm is cavity dumped to produce ~10 ps pulses with a pulse energy of ~6 nJ/pulse. The repetition rate of the dye laser was selected to be at least 5 times the natural lifetime of the sample (475 kHz for measurements at 780 nm or 190 kHz for measurements at 640 nm). The beam passes through an iris and illuminates, without focusing, a 10 mm quartz cuvette containing the sample. The emitted light is collected at 90 ° and focused onto the slit of a 240 mm focal length, single grating monochromator and subsequently delivered to a cooled, multichannel plate-photomultiplier tube (MCP, Hamamatsu R3809U-51). The intensity of the detected luminescence is varied by use of neutral density filters mounted before the monochromator. The signal from the MCP is amplified prior to sending it into a 200 MHz constant fraction discriminator (CFD, Tennelec 454) whose output serves as the start pulse for a time-to-amplitude converter (TAC, Tennelec 864). The stop pulse is obtained by focusing 10% of the excitation beam onto a Si: PIN photodiode, whose output is sent into a variable delay box, then to a CFD, and finally to the TAC. The TAC's output is sent to a multichannel analyzer that is interfaced to a PC. The instrument response of the apparatus is 80 ps at the fwhm.

III. Results and Discussion

The energy migration process is initiated by photoexcitation of one of the Ru monomers to a singlet metal-to-ligand charge transfer (^{1}MLCT) state, which is followed by efficient inter-

(74) Maxwell, K. A. Doctoral Dissertation, University of North Carolina at Chapel Hill, Chapel Hill, NC, 1999.
(75) Demas, J. N.; Crosby, G. A. *J. Phys. Chem.* **1971**, *75*, 991.
(76) Casper, J. V.; Meyer, T. J. *J. Am. Chem. Soc.* **1983**, *105*, 5583.
(77) Casper, J. V.; Kober, E. M.; Sullivan, B. P.; Meyer, T. J. *J. Am. Chem. Soc.* **1982**, *104*, 630.

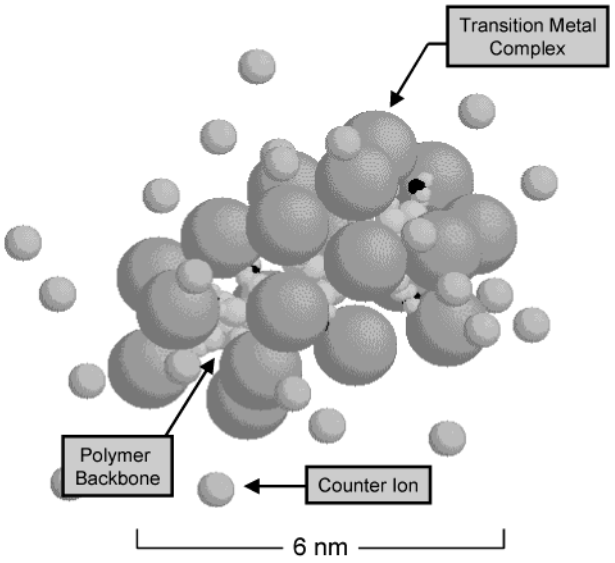

Figure 2. Structure of a polymer assembly containing 20 transition metal complexes calculated by Monte Carlo simulations (see text). Large spheres represent the metal complexes and small spheres are the PF_6^- counterions.

system crossing to a ^{3}MLCT state in a matter of several hundred femtoseconds.[78,79] The lifetime of this low-lying triplet state is about 1000 ns, and as a result there is sufficient time for the excited state to either transfer to an adjacent Ru complex or be quenched by direct energy transfer to a lower energy Os site before relaxation back to the ground state. Because the Os excited state lies approximately 0.34 eV below the Ru excited state, the Os sites are considered to be deep traps that terminate the energy migration process.

This work focuses on polymers with mixed Ru/Os loading ($PS\text{-}Ru_{17}Os_3$), their corresponding ruthenium and osmium homopolymers ($PS\text{-}Ru_{20}$ and $PS\text{-}Os_{20}$), and the two monomer complexes, $Ru(dab)_2(mab)^{2+}$ and $Os(bpy)_2(mab)^{2+}$. The homopolymers and monomer complexes serve as reference systems.[80] This approach is justified by a series of spectroscopic experiments that indicate the polymers are well described as a collection of chromophores whose excited states remain intact upon incorporation into the array. Thus, the polymer backbone is primarily a structural support that holds complexes in close proximity.

The outline of this section is as follows. In Section A we address some of the issues associated with the polymer structure and the arrangement of the metal complexes. These concepts are central to the interpretation of the spectroscopic data, and thus the salient details are presented early in the discussion. The steady-state spectroscopy is discussed in Section B and the time-resolved experiments are presented in Section C. In that section we discuss the kinetics of the energy transfer process, measurements of the sensitization efficiency, and the energy transfer mechanism. Finally in Section D we describe the Monte Carlo simulations that are used to model the polymer structure and gain insight into the intrinsic properties of the energy migration dynamics.

(78) Demas, J. N.; Crosby, G. A. *J. Am. Chem. Soc.* **1971**, *93*, 2841.
(79) Damrauer, N. H.; Cerullo G.; Yeh, A.; Boussie, T. R.; Shank, C. V.; McCusker, J. K. *Science* **1997**, *275*, 54−57.
(80) Other possible choices for the homopolymer systems are $PS\text{-}Ru_{17}$ and $PS\text{-}Os_3$. However, the macromolecular structure is strongly influenced by the number of metal complexes, and therefore these systems ($PS\text{-}Os_3$ in particular) will more than likely have very different structures when compared to their $PS\text{-}Ru_{17}Os_3$ parent. This would make them poor mimics for the mixed-loaded polymer.

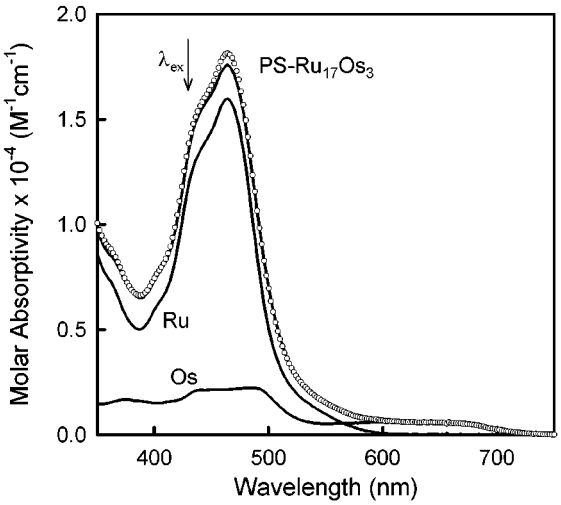

Figure 3. Absorption spectra of the $PS\text{-}Ru_{17}Os_3$ polymer assembly and Ru and Os monomer complexes, $Ru(dab)_2(mab)^{2+}$ and $Os(bpy)_2(mab)^{2+}$, in room temperature CH_3CN. The monomer spectra are scaled by 17/20 and 3/20, respectively, to reflect their contributions to the polymer sample. The solid lines are the experimental observation; the individual points are obtained by the addition of the two monomer spectra. The arrow identifies the excitation wavelength used for the time-resolved experiments discussed later in the text.

A. Supramolecular Structure and Metal Complex Loading. The microscopic details of the energy transfer dynamics will depend on the polymer structure and this is greatly influenced by the large (14 Å diameter) metal dication monomer units. A typical structure calculated from molecular modeling is depicted in Figure 2 (the details of these calculations are described later). The larger spheres are the Ru(II) or Os(II) chromophores and the smaller spheres are the PF_6^- counterions that surround the polymer whose overall charge is +40. The densely loaded polymer adopts a twisted backbone and extended rodlike structure to alleviate the steric and Coulombic repulsions between adjacent chromophores. One consequence of the dense loading is that the average distance between the peripheries of adjacent chromophores is 2−3 Å. It is this close proximity of the complexes that is partly responsible for the efficient energy transfer that is observed.

The arrangement of the Ru and Os complexes on the polymer chain plays an integral role in the description of the migration dynamics. The mixed polymer is loaded with (on average) 17 Ru and 3 Os complexes. The average, however, is over the entire sample not an individual chain. And furthermore, the loading is random, allowing for a certain fraction of chains to have more or less Os complexes in a number of possible configurations. The probability that a chain will have n Os sites is given by,

$$P_n = \frac{N!}{(N-n)!n!} \cdot P_{\mathrm{Ru}}^{(N-n)} \cdot P_{\mathrm{Os}}^{n} \qquad (2)$$

where P_{Ru} (17/20) and P_{Os} (3/20) are the probability that a given site is Ru or Os, respectively, and N is the total number of complexes. For our samples there is a narrow distribution of chain lengths (PDI = 1.08) centered at $N = 20$. Statistically we expect 24% of the chains to have three Os with 35% of the chains having more than three and 41% having less; 4% of the chains are expected to be Ru homopolymer (i.e. $n = 0$).

B. Steady-State Spectra. The ground-state absorption spectrum of the $PS\text{-}Ru_{17}Os_3$ polymer is displayed in Figure 3. The spectrum shows an intense band centered at 450 nm and a

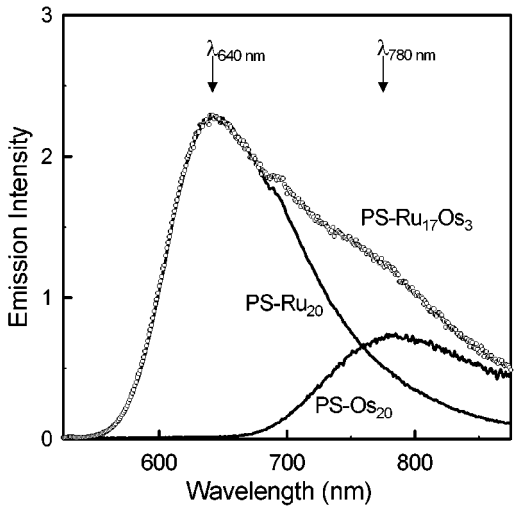

Figure 4. Emission spectra of PS-$Ru_{17}Os_3$ (open circles) and its Ru and Os homopolymer counterparts (solid lines). The arrows indicate the two monitoring wavelengths used in the time-resolved experiments. Emission monitored at 640 nm arises entirely from Ru(II) luminescence, while the emission monitored at 780 nm has both Ru(II) and Os(II) contributions (see text).

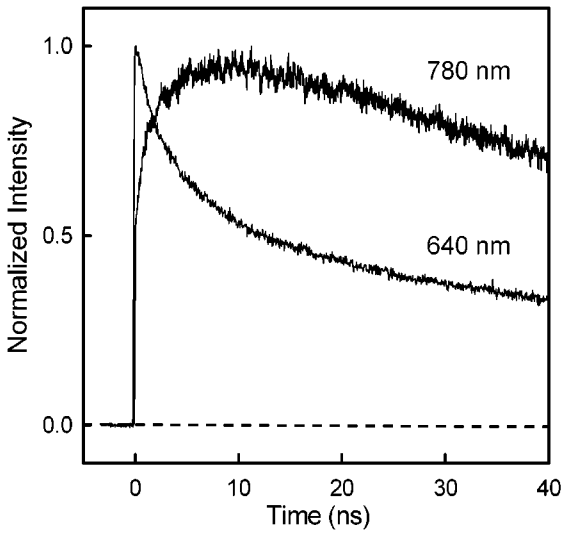

Figure 5. Time-resolved emission from PS-$Ru_{17}Os_3$ detected at 640 (entirely Ru(II)) and 780 nm (primarily Os(II)). Excitation was at 430 nm. Both transients are normalized such that their maximum intensity is equal to unity.

weaker absorption that extends out to about 700 nm. The polymer spectrum can be understood in terms of the absorption spectra of the two monomer complexes, $Ru(dab)_2(mab)^{2+}$ and $Os(bpy)_2(mab)^{2+}$. These spectra are also shown in the figure, but their absorptivities are weighted by 17/20 and 3/20, respectively, to reflect their relative abundances within the polymer sample.

The broad absorption band centered near 450 nm (for both Ru and Os) is a metal-to-ligand charge transfer (MLCT) transition that involves the promotion of a metal dπ electron to a π^* orbital on one of the polypyridyl ligands. Any of the three ligands could receive the electron in the optical excitation process, but at long times the photoexcited electron resides on the lowest energy ligand, i.e. one of the two *dab* ligands.

On a per molecule basis, the absorption cross-section for excitation of the Ru complex at 430 nm (the excitation wavelength used in these experiments) is comparable to that of Os. As a result, the relative probability for Ru or Os excitation is determined by their mole fractions in the sample. In addition to the 450 nm band, the Os complex has a weak absorption feature centered around 630 nm. This transition corresponds to direct excitation to a ^{3}MLCT state. Although this is formally a spin-forbidden transition, its intensity becomes appreciable in Os as a result of the large spin−orbit coupling in the heavier metal.

The absorption spectrum of the polymer can be reproduced by a superposition of the weighted monomer spectra. This suggests that the polymer can be described as an array of weakly coupled chromophores whose electronic structures remain essentially intact upon loading onto the polymer backbone. This conclusion is also supported by other general observations. At low excitation energies, the spectroscopic signatures (i.e. absorption spectra, emission spectra, and excited-state lifetimes) exhibited by the Ru and Os homopolymers are almost identical to their monomer counterparts.

Displayed in Figure 4 is the emission spectrum of PS-$Ru_{17}Os_3$ in room temperature CH_3CN. The spectrum shows two features: a high-energy band with a maximum at 640 nm, and a low-energy shoulder in the vicinity of 750−800 nm. These features are assigned to Ru- and Os-complex emission, respectively. The emission spectra of the two homopolymers are also displayed in the figure, with their intensities scaled to reflect their relative contributions to the PS-$Ru_{17}Os_3$ emission.

The relative intensities of Ru and Os emission offer evidence of extensive quenching of the Ru excited state. The ratio of the two emission intensities is determined by the number of Ru excited states, the number of Os excited states (created by either direct excitation or Ru*→Os energy transfer), and the relative luminescence quantum yields. The steady-state emission spectrum shows that Ru emission is about 3 times more intense than that of Os. However, the quantum yield for Ru emission is ≈10%, or about 30 times larger than that of Os ($\Phi = 0.32\%$). Once adjusted for the difference in quantum yields, the relative intensities suggest that the Os excited states outnumber the Ru excited states by a factor of 10. Since there are 5−6 times more Ru excited states produced by photoexcitation, the presence of a larger number of excited Os complexes points to an efficient Ru*→Os energy transfer process. Measurements of the energy transfer efficiency (Section C-2) support this conclusion. In fact, the majority of the Ru complex emission observed in the PS-$Ru_{17}Os_3$ spectrum is attributed to polymer chains that have zero Os complexes, i.e. Ru homopolymers. Statistically, such chains are expected to constitute 4% of the polymer sample.

C. Energy Transfer Dynamics. Photoinduced energy migration is followed through the time-resolved luminescence detected at 640 and 780 nm, both of which are displayed in Figure 5. At 640 nm Ru is the sole emitter. The emission at this wavelength decays on multiple time scales, ranging from 2 to 980 ns. The emission detected at 780 nm reflects the appearance of Os(II) excited states. The growth in emission at this wavelength shows a rapid rise followed by a slower rise to the maximum at 5−10 ns. The rapid rise accounts for 56% of the maximum intensity and lies within the instrument response of the apparatus (80 ps). The slower rise coincides with the fastest decay component in the Ru emission, implying that the slower growth arises from the production of Os excited states by Ru*→Os energy transfer. The decay of the luminescence after the maximum is nonexponential. This differs from PS-Os_{20}, which decays with single exponential kinetics and a 49 ns lifetime. The nonexponential behavior observed in the decay of the 780 nm emission is

probably the result of photosensitization events that are delayed due to Ru*→Ru energy migration.

The Ru emission past 500 ns decays with a lifetime of 980 ns, which is characteristic of the PS-Ru_{20} homopolymer (1000 ns). One possible explanation of this is that the Ru excited state gets trapped within a subset of complexes and is not able to fully explore the entire polymer. Although such a scenario cannot be entirely ruled out, our simulations of the energy migration dynamics (Section D) do not support its presence. Instead we attribute the long tail in the Ru luminescence to emission from the subset of polymer chains that do not have any Os complexes, i.e. Ru homopolymer, which is present in the mixed polymer sample due to the statistical nature of the metal complex loading.

The deviation from single-exponential kinetics in both the Ru and Os data is a result of a complex energy transfer process where the number of Ru*→Ru migration steps that precede Ru*→Os trapping varies from one excitation event to the next. As mentioned earlier, the average ratio of Ru to Os over the ensemble of chains is 17:3 but the loading on an individual chain is random. This results in a distribution in the degree of Os loading and a large number of possible chromophore configurations. Furthermore, since an energy gradient toward the trapping site does not exist, the propagation of the excited state from one Ru to the next is a series of uncorrelated hopping events. As a result, even if two polymer chains have exactly the same arrangement of chromophores and the same initial location of the excited state, the random walk behavior could cause the path that one excited state takes to the trap to be different from another.

The growth in the Os emission intensity and the concomitant decay in the Ru emission most certainly reflect the rates of excited state energy transfer. However, because the observed time scales are closely linked to the degree of Os loading they do not provide a direct measure of the energy transfer times. For example, a chain with a 16:4 Ru to Os loading would show a faster growth rate in the Os emission simply because a Ru excited state would make on average fewer steps to the Os trap. Since the Ru*→Ru energy transfer time should be independent of the number of Os complexes on a given chain, the growth and decay times extracted directly from the data can, at best, provide only a qualitative description of the energy migration process. In the sections that follow, we present a more thorough analysis of the spectroscopic data, and develop a fundamental picture of the energy migration dynamics.

1. Time-Resolved Data—A Closer Look. There are two contributions to the luminescence at 780 nm that do not arise from Os sensitization. These are (1) emission originating from Os centers directly excited by the laser,and (2) Ru luminescence that is also detected due to the overlap of Ru and Os emission bands. The question therefore arises as to which features of the 780 nm transient are due to energy migration and which aspects are not.

The contributions to the transient emission that do not arise from sensitized emission are easily determined. The contribution from direct Os excitation is assessed by comparing the PS-Ru_{17}-Os_3 transient at 780 nm with that of PS-Os_{20} under the exact same conditions of concentration and integrated irradiance. The Ru contribution is determined by exploiting the difference in Ru and Os emission lifetimes. PS-Ru_{20} has an emission lifetime of 1000 ns, which is substantially longer than the 49 ns lifetime observed for PS-Os_{20}. Thus, the 780 nm luminescence observed at very long times (i.e. >500 ns) is due solely to Ru. Its contribution is determined by scaling the emission transient observed at 640 nm to match the 780 nm data at times greater than 500 ns. This assumes that the decay of the Ru emission detected at 780 nm has the same shape as that at 640 nm (where Ru is the sole emitter). This assumption is supported by time-resolved emission experiments performed on PS-Ru_{20} that show no spectral shifts in the decay of the Ru emission band, indicating that it decays uniformly. The sum of these two contributions is displayed along with the total emission detected at 780 nm in Figure 6.

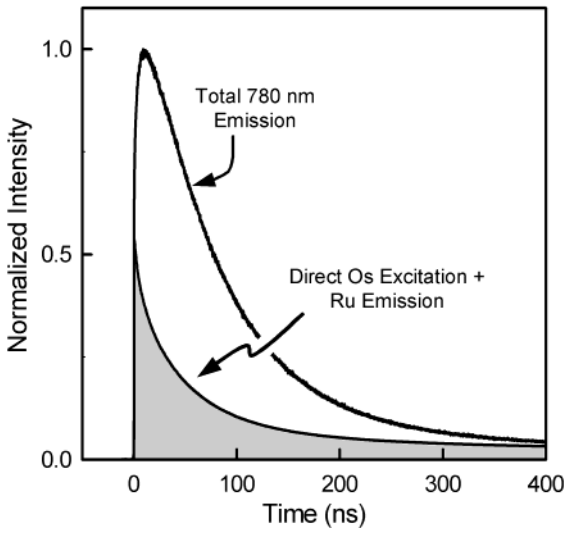

Figure 6. Contributions from direct Os excitation and Ru emission to the total PS-$Ru_{17}Os_3$ emission detected at 780 nm. The total emission at 780 nm is the same as that displayed in Figure 5, only on a longer time sale.

The sensitized Os emission is determined simply by subtracting out the direct Os excitation and Ru contamination contributions from the total emission. It represents a substantial fraction (≈60%) of the total luminescence detected at 780 nm. In the next section, we will use this to determine the efficiency of Os sensitization.

The rise in the *sensitized* emission is displayed in the top panel of Figure 7. This portion of the transient cannot be fit by a single-exponential model, which is evidenced by the residuals (Figure 7). The rise is well described, on the other hand, by a biexponential function of the form,

$$I(t) = A_1\left(1 - \exp\left(-\frac{t}{\tau_1}\right)\right) + A_2\left(1 - \exp\left(-\frac{t}{\tau_2}\right)\right) \quad (3)$$

The fit to this function is displayed as the solid line in the top panel of Figure 7. The rise is comprised of a fast, 400 ps component, which accounts for about 25−30% of the maximum amplitude, and a slower component with a 3.6 ns time constant. The fit to a biexponential function is not meant to imply that the polymer system should be viewed as a two-state system, which it most certainly is not. Nevertheless, the presence of two kinetic components suggests that there are two qualitatively distinct dynamical processes occurring on different time scales. The 400 ps component is attributed to the prompt Ru*→Os energy transfer that occurs when the Ru excited state is formed at a site directly adjacent to the Os trap. As mentioned earlier, the Ru*→Os energy transfer will take place on a range of time scales. The fast time component observed here probably represents the fastest portion of the distribution, since it is these energy transfer events that will give rise to prompt sensitization.

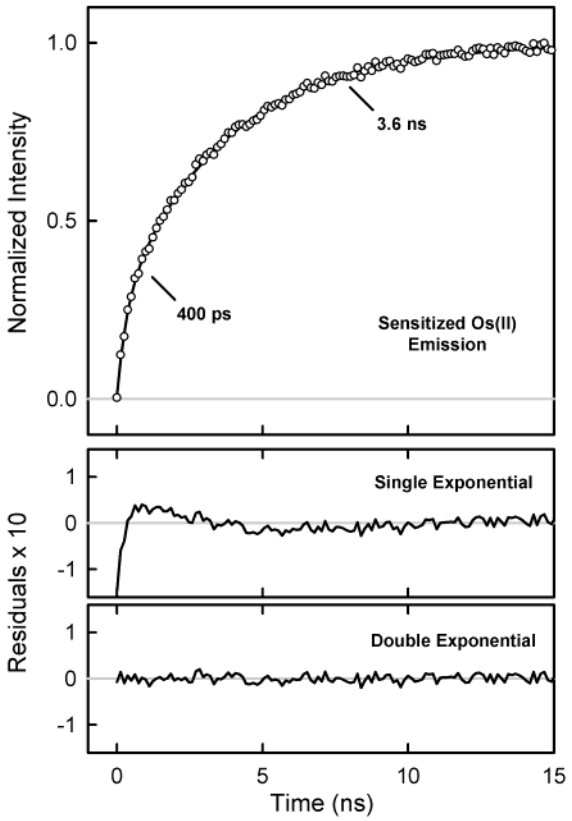

Figure 7. The upper panel shows rise in sensitized Os(II) emission from PS-$Ru_{17}Os_3$ detected at 780 nm. The individual points are the experimental data and the solid line is the result of a nonlinear least-squares fit to a biexponential function. Attempts were made to fit the rise to a single-exponential function. The residuals from this fit (middle panel) show clear deviation from single-exponential behavior. The residuals displayed in the lowest panel are for the biexponential fit. The sum-of-squared residuals are 0.06 and 0.01 for the single exponential and biexponential fits, respectively.

The rest of the rise is attributed to emission from sensitized Os complexes that are formed after one or more Ru*→Ru hops. A more realistic model of the energy migration dynamics is incorporated into our Monte Carlo simulations, which are discussed in Section D.

2. Efficiency of Sensitizing Os Traps. Energy transfer competes with the intrinsic radiative (k_r) and nonradiative (k_{nr}) pathways in depopulating the excited state of the donor. The quantum yield, or efficiency (χ_{EN}), of sensitizing the Os(II) sites can be defined as,

$$\chi_{EN} = \frac{k_{EN}}{k_{EN} + k_r + k_{nr}} = 1 - \frac{\Phi_D}{\Phi_D^o} = 1 - \frac{\tau_D}{\tau_D^o} \qquad (4)$$

Thus, quantum yield (Φ) or lifetime (τ) measurements of the donor in the presence (Φ_D or τ_D) and absence (Φ_D^o or τ_D^o) of the acceptor can be used to calculate χ_{EN}. The quantum yields for Ru emission from PS-$Ru_{17}Os_3$ and PS-Ru_{20} polymers are 0.019 and 0.1, respectively, implying a sensitization efficiency of 80 ± 10%.

Alternatively, the efficiency can be defined as the ratio of the number of sensitized acceptors, denoted $N(Os_{EN})$, to the number of excited donors, i.e.

$$\chi_{EN} = \frac{N(Os_{EN})}{N(Ru^*)} \qquad (5)$$

Both of these quantities can be determined by using the luminescence decay data of the acceptor.

The first quantity needed is $N(Os_{EN})$, the number of Os excited states formed via sensitization. This is given by,

$$N(Os_{EN}) = \frac{G}{\Phi_{Os}}\left(\eta_S - \eta_R \cdot \frac{[S]}{[R]} \cdot P_{Os}\right) \qquad (6a)$$

where η is an integrated intensity obtained from the emission transient, i.e., $\eta = \int I(t)\, dt$. η_S and η_R are the total number of photons observed at 780 nm from PS-$Ru_{17}Os_3$ (sample) and PS-Os_{20} (reference), respectively. (The Ru contribution is removed from the mixed polymer emission prior to performing this analysis.) Φ_{Os} is the emission quantum yield of PS-Os_{20} in CH_3CN, P_{Os} is the mole fraction of Os in the sample (3/20), and G is a geometrical factor that reflects the photon collection efficiency of our apparatus at 780 nm. The ratio [S]/[R] accounts for differences in polymer chain concentration between the sample and reference: this is determined from absorption measurements on the two separate samples. The first term in eq 6a is the total number of Os excited states produced by either sensitization or direct excitation, while the second term reflects the number of Os excited states resulting from direct excitation alone.

The second quantity needed is $N(Ru^*)$, the number of directly excited donors. This is determined from the PS-Os_{20} reference by using the following expression,

$$N(Ru^*) = G\left(\frac{\eta_R}{\Phi_{Os}} \cdot \frac{\epsilon_{Ru}}{\epsilon_{Os}} \cdot \frac{[S]}{[R]} \cdot P_{Ru}\right), \qquad (6b)$$

where ϵ is the molar absorptivity at the excitation wavelength for Ru and Os, and P_{Ru} is the mole fraction of Ru in the sample (17/20). The ratio of absorptivities is included to take into account the difference in excitation probabilities of the Ru and Os complexes. In essence, the Os homopolymer is used as a quantum counter. In principle the Ru emission could be used, but this would introduce the Ru quantum yield into the analysis as well as the photon collection efficiency at 640 nm. Not only is this avoided by using the Os emission, but since Φ_{Os} and G appear in both eqs 6a and 6b, they do not appear in the final expression for the efficiency (eq 5). The efficiency of Os sensitization in the PS-$Ru_{17}Os_3$ polymer at room temperature in CH_3CN is calculated in this manner to be 88 ± 12%.

On the basis of these two methods we estimate the overall efficiency for the sensitization of the Os traps to be approximately 85%. We point out, however, that this represents an average efficiency over the entire sample, including those chains that do not have any Os complexes and hence remain unquenched. Depending upon the fraction of PS-Ru_{20} homopolymer in the sample, the sensitization efficiency for the subset of chains with at least one Os complex could be substantially higher.

The presence of PS-Ru_{20} in the sample is expected, and due in part to the statistical nature of the loading. Statistical arguments predict a 4% fraction of homopolymer. However, the actual fraction appears greater than this. The homopolymer contribution is seen most clearly in the long time decay of the 640 nm emission, Figure 8. The longest time component is assigned to emission from the homopolymer fraction. Extrapolating this emission tail back to $t = 0$ we find that 85% of the integrated emission at 640 nm can be attributed to Ru homopolymer. The fraction of homopolymer

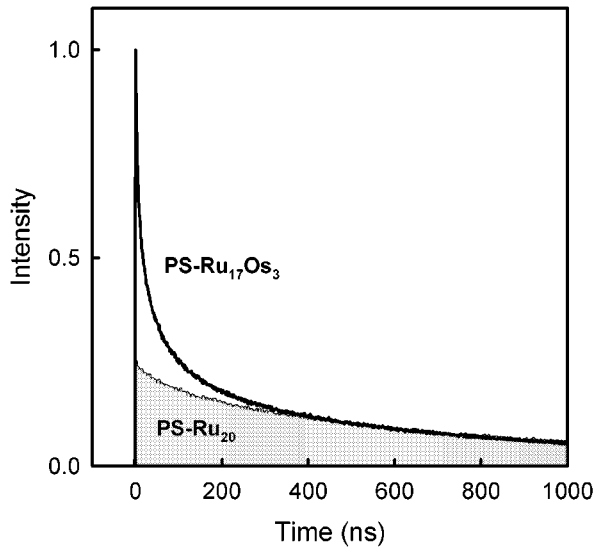

Figure 8. Time-resolved emission from PS-$Ru_{17}Os_3$ detected at 640 nm. The shaded area depicts the contribution from the Ru hompolymer.

chains (F_H) is given by

$$F_H = \frac{N_H}{N_T} = \left(\frac{\eta_H}{\eta_T}\right)(1 - \chi_{EN}) \qquad (7)$$

where N_H and N_T are the number of homopolymer chains and the total number of chains, respectively, and η_H and η_T represent the integrated emission intensities. The ratio η_H/η_T is the fraction of the total emission that emanates from the homopolymer chains, 85%. The homopolymer fraction thus calculated is 10−12%. It is unclear why there is a larger fraction than statistically predicted. It is perhaps due to an artifact of the synthetic procedure, arising from the limited solubility of the amine-derivatized polymer precursor. The implication is that the sensitization efficiency averaged over the entire sample can be at most 90%, and thus the efficiency of those polymer chains that have at least one Os complex is in fact closer to 95%. We point out that deviation from the statistics of eq 2 does not affect any of the numerical results achieved thus far. The analysis of the steady-state spectra and the efficiency of energy transfer depend only upon the relative amounts of Ru(II) and Os(II) complexes in the sample, not on how they are distributed among the chains.

3. Energy Transfer Mechanism. The energy transfer rate constant can be cast in a "golden-rule" expression in which k_{EN} is proportional to the square of an electronic coupling matrix element, H_{DA}.[15,81] This two-electron matrix element involves the molecular orbitals on both the donor and acceptor. The electronic factor can be split into a Coulombic term and an exchange term, which give rise to Förster and Dexter energy transfer mechanisms, respectively.

The Förster mechanism describes energy transfer through a dipole−dipole coupling term. As a result, the rate constant has a gradual dependence ($1/R^6$) on the donor−acceptor separation, and energy transfer is capable of occurring over large distances. The Förster mechanism is most efficient when the optical transitions connecting the ground and excited states in both partners are electric-dipole allowed.[82] On the surface this would seem to exclude the Förster mechanism for energy transfer involving Ru and Os metal complexes, where optical transitions to the lowest excited state are spin-forbidden. However, because of the large spin−orbit coupling, this selection rule may not be absolute. Spin−orbit coupling introduces some singlet character into the emitting states. The fraction is estimated to be less than 11% in $Ru(bpy)_3^{2+}$, and in $Os(bpy)_3^{2+}$ it is probably around 30%.[83] Although we cannot completely rule out the Förster mechanism, the small percentage of singlet character in the donor and acceptor complexes suggests that it may not be the dominant pathway.

The Dexter mechanism, on the other hand, involves the exchange of donor and acceptor electrons, and is therefore expected to operate only at short distances where the electron clouds can interpenetrate. Because this interaction requires overlap between the orbitals, the energy transfer rate constant in the Dexter formulation falls off exponentially with increasing separation. The distance over which energy transfer occurs can be extended, however, when the donor and acceptor are connected through a series of covalent bonds. In these cases the orbitals can indirectly mixed via a superexchange type interaction that involves molecular orbitals on the intervening bonds. The polymer backbone in PS-$Ru_{17}Os_3$ is in essence a bridging ligand between adjacent complexes, and hence there is the potential for a through-bond pathway. Thus the question is whether the coupling between the sites arises from a direct overlap of wave functions or a bridge-mediated superexchange pathway.

There are clear examples in the literature of efficient through bond coupling in Ru/Os dimers. Harriman and co-workers[84] report an energy transfer time of 6 ps for the complex $[(bpy)_2Ru(bpy\text{-}C{\equiv}C\text{-}bpy)Os(bpy)_2](PF_6)_4$. Although the observation is interesting, the short bridging length and high degree of conjugation make comparisons to this system irrelevant. For energy transfer to proceed through bond in our system, efficient coupling would need to occur across a network consisting of 18 σ and π bonds. Reports of Ru*→Os energy transfer in systems involving extended bridges have also appeared in the literature. Balzani et al.[85] observe a 1.5 ns energy transfer time for $[(bpy)_2Ru(bpy\text{-}(ph)_3\text{-}bpy)Os(bpy)_2]^{4+}$, where the bridge is 11 Å and 13 bonds in length. Here energy transfer is attributed to a through-bond-type mechanism, which is probably enhanced by the high degree of conjugation in the phenylene spacers. This is in contrast to the $[(bpy)_2Ru(bpy\text{-}S\text{-}bpy)Os(bpy)_2]^{4+}$ dimer, where S consists of a bicyclooctane component linked to two ethylene components.[86] This bridging ligand is roughly 9 Å in length, and unlike the previous case, the bicyclooctane bridge contains no conjugated bonds. The saturated bonds substantially diminish the electronic communication between metal centers, leading to a longer time scale for energy transfer compared to the phenylene bridge, despite its physically shorter length. The range of energy transfer rate constants observed in various dimers reflects the differences between bridging ligands in their ability to mediate electronic communication between the donor and acceptor. Thus, the most germane comparisons will be those that have similar bonding networks between the metal centers.

Schmehl and co-workers[87] provide an example of a bridging ligand that more closely resembles the combination of σ and π bonds found in our polymer. They report an energy transfer time of about 10 ns in $[(dmb)_2Ru(bpy\text{-}etphet\text{-}bpy)Os(dmb)_2]^{4+}$

(81) Speiser, S. *Chem. Rev.* **1996**, *96*, 1953−1976.
(82) Förster, T. *J. Chem. Soc., Faraday Trans.* **1959**, *27*, 7.
(83) Kober, E. M.; Meyer, T. J. *Inorg. Chem.* **1984**, *23*, 3877−3886.
(84) Harriman, A.; Romero, F. M.; Ziessel, R.; Benniston, A. C. *J. Phys. Chem. A* **1999**, *103* (28), 5399−5408.
(85) Schlicke B.; Belser, P.; Cola, L. D.; Sabbioni, E.; Balzani, V. *J. Am. Chem. Soc.* **1999**, *121* (17), 4207−4214.
(86) De Cola, L.; Balzani, V.; Barigelletti, F.; Flamigni, L.; Zelewsky, A.; Frank, M.; Vögtle, F. *Inorg. Chem.* **1993**, *32*, 5228.
(87) Shaw, J. R.; Sadler, G. S.; Wacholtz, W. F.; Ryu, C. K.; Schmehl, R. H. *New J. Chem.* **1996**, *20*, 749−758.

where the bridge spans roughly 12 Å and 9 bonds. The Ru*→Os energy transfer observed in this system is slower than that found in our polymer (~400 ps), despite the fact that there are fewer bonds in its bridging network. This trend is inconsistent with a through-bond-type mechanism.

It is consistent with an energy transfer mechanism that arises from a direct overlap of the donor and acceptor wave functions. The distance between Ru and Os complexes in the dimer will be very different than that found in the polymer. The dimer will probably adopt an extended structure that minimizes the Coulombic repulsions between the metal complexes. In contrast, our Monte Carlo simulations (Section D) suggest that the dense loading of the polymer leads to Ru and Os complexes that are in much closer proximity, despite the longer bridging network between them. This suggests that energy transfer in the polymer is due, at least in part, to an effective coupling between adjacent chromophores that does not involve the orbitals on the bridging network. While this tends to rule out coupling through the polymer backbone, there is also the possibility of a superexchange pathway involving the intervening solvent. Solvent-mediated superexchange has been discussed in relation to energy transfer in other systems.[81]

D. Monte Carlo Simulation of Energy Migration. The energy transfer time will be characterized not by a single rate constant but rather a distribution of rate constants that reflects a range of separations between metal complexes. Thus, to determine the time scale for Ru*→Ru and Ru*→Os energy transfer, the physical model must incorporate a microscopic description of the polymer's structure. The kinetic model used here combines a Monte Carlo simulation that yields structural information with a stochastic simulation of the energy migration. Together with the time-resolved measurements these calculations provide insight into the structure and dynamics at the molecular level.

1. Polymer Structure. The polymer structure is calculated by using a Metropolis Monte Carlo algorithm. The potential energy function that describes the assembly represents each metal complex as a hard 14 Å diameter sphere with a +2 charge placed at its center. The polystyrene backbone is modeled as a flexible chain that is free to rotate about the C−C single bonds (whose lengths are held constant). The surrounding solvent is treated as a dielectric continuum and the PF_6^- counterions are represented by hard spheres (6.3 Å diameter) with a −1 charge located at their centers. Our calculations are performed on polymer chains in which every binding site is occupied by a metal complex. This is consistent with ^{1}H NMR measurements that indicate complete loading of the polymer chains.

The initial structure is constructed by placing the metal complexes on the side chains of an extended polystyrene chain. Because polystyrene is considered to have an atactic structure, the handedness of the chiral carbons in the backbone is chosen at random such that right- and left-handed sites are equally likely. Starting with this structure, one C−C bond in the polymer backbone is chosen at random. The array structure is altered by rotation about this bond and the change in energy, ΔE, between the old and the new configurations is calculated. If the energy of the new structure is lower, the move is accepted. If the potential energy is increased, the new configuration is accepted only if the quantity $\exp(-\Delta E/k_BT)$ is less than a random number chosen on the interval (0,1). The structure is annealed during the course of generating 5×10^5 configurations. After this annealing period an additional 10^6 structures are generated, from which 20 are selected. This is repeated 20 times to produce an ensemble of 400 structures.

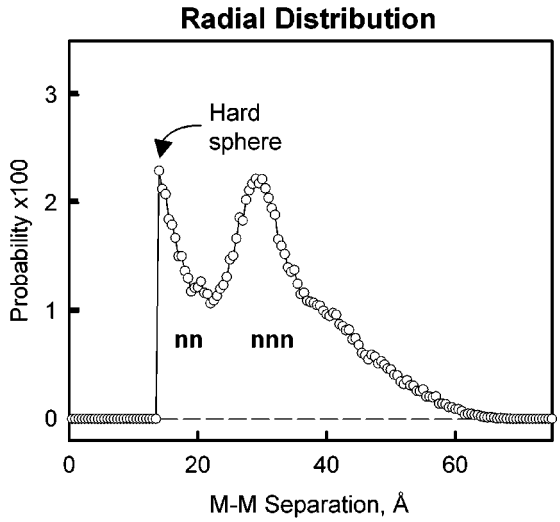

Figure 9. Metal−metal pair distribution function calculated from Monte Carlo simulations of the polymer structure. nn and nnn refer to the nearest neighbors and next nearest neighbors, respectively.

A typical structure is shown in Figure 1. The large spheres represent the transition metal complexes while the smaller spheres represent the PF_6^- counterions. The carbon backbone undergoes significant twisting to relieve the steric and Coulombic repulsion between the large transition metal complexes. The result is a structure in which one complex is in close proximity to several others within the array. In addition, the nearest neighbor through space is not necessarily the same as the nearest neighbor through bond.

The metal−metal (MM) pair distribution function obtained from analyzing 400 different chain structures is displayed in Figure 9. The largest MM separation with nonzero probability is around 6 nm, reflecting the average length of the polymer chain. The oscillations in the probability distribution indicate the presence of structural organization that is analogous to the level of order found in other ostensibly disordered systems such as molecular liquids. Each oscillation in the pair distribution corresponds to a "chromophore shell" that surrounds the metal complex of interest. There are two distinct shells observed in the distribution, one centered at 14 Å and the other at 29 Å. These two peaks correspond to the distribution of nearest neighbors (nn) and next-nearest neighbors (nnn), respectively. From the integrated area of the nearest neighbor (nn) peak, we estimate that each complex has between 4 and 5 nearest neighbors and that in more than half of the nearest neighbor pairs the peripheries of the complexes are separated by less than 2 Å.

2. Simulation of Energy Migration Dynamics. We have extended our Monte Carlo simulations of the polymer structure to model the excited-state energy migration dynamics. Similar methods have been implemented to simulate energy migration in other systems.[38,88] The output of the computer model is an emission transient that is directly comparable to our experimental data, and thus there is a direct link between the simulations, which provide insight into the dynamics at the molecular level, and the experimental observations. The simulations start with a structure selected at random from a 300 K thermal ensemble generated by the Monte Carlo simulation. Each site is randomly assigned to be either a Ru or Os complex with a probability of 17/20 and 3/20, respectively. To be consistent with the experiment, the PS−Ru_{20} homopolymer fraction is set to be 10%.

(88) Hisada, K.; Ito, S.; Yamamoto, M. *Langmuir* **1996**, *12*, 3682−3687.

The macro structure of the polymers is such that there is a range of separations between adjacent complexes, and thus the Ru*→Ru and Ru*→Os energy transfer steps are not described by a single rate constant, but rather a distribution of rate constants. For a given polymer structure and Ru/Os loading configuration, the rate constants for energy transfer between pairs of metal centers are calculated based on the physical separation between the complexes, i.e.

$$k_{ij}^{Ru}(R_{ij}) = k_o^{Ru} \exp(-\beta_{Ru} R_{ij}) \quad (8a)$$

$$k_{ij}^{Os}(R_{ij}) = k_o^{Os} \exp(-\beta_{Os} R_{ij}) \quad (8b)$$

where the first and second expressions apply to Ru*→Ru and Ru*→Os energy transfer, R_{ij} is the separation between site i and site j, k_o is the rate constant at closest contact, and β is an attenuation parameter. This definition assumes that the electronic coupling between the donor and acceptor arises from a direct orbital overlap.

A migration "trajectory" is started by randomly choosing one of the metal sites as the initial location of the excited state. Each trajectory is comprised of a series of steps in which a Ru excited state either hops to another site (with a rate constant of k_{ij}^{Ru} or k_{ij}^{Os}) or decays to its ground state at a rate given by the Ru excited-state lifetime, k_{em}^{Ru}. Each step is calculated by using a stochastic kinetic algorithm adapted from Gillespie,[89] the details of which are presented in the Appendix. Once energy transfer to an Os site occurs, energy migration is halted (i.e. Os*→Ru energy transfer is not allowed), and the Os excited state decays to the ground state at a rate given by the Os emission lifetime, k_{em}^{Os}. About 5 million trajectories are calculated starting with different chain structures and Ru/Os loading configurations.

There are six rate constant parameters that enter into the simulation: k_0^{Ru}, k_0^{Os}, β_{Ru}, β_{Os}, k_{em}^{Ru}, and k_{em}^{Os}. The last two parameters, the Ru and Os complex emission rates, are measured in separate experiments on the PS-Ru_{20} and PS-Os_{20} homopolymers to be 1000 and 49 ns, respectively. In the simulation these are treated as fixed parameters. The attenuation parameters, β_{Ru} and β_{Os}, reflect the decrease in the exchange integral with increasing donor−acceptor distance. The attenuation parameters for Ru*→Ru and Ru*→Os are expected to be similar to each other, and thus for simplicity the two are taken to have the same value, i.e. $\beta_{Ru} = \beta_{Os} = \beta$. Although we do not know the exact value for the attenuation parameter, we can identify a typical range of values based on studies of energy transfer in other systems.

In many instances the magnitude of β has been estimated based on the distance dependence of the through-space energy transfer rate constants. Yamamoto and co-workers[88,90−92] investigated methylene-linked donor−acceptor complexes based on organic chromophores embedded in frozen solutions, polymethyl-methacrylate (PMMA) resins, and Langmuir−Blodgett films. They find β for *intramolecular* energy transfer to be in the neighborhood of 1.7−2.1 Å^{-1}, which is quite similar to the attenuation parameters measured for *intermolecular* energy transfer in similar materials.[93,94] There are also examples in the literature involving donor−acceptor assemblies based on transition metal coordination complexes. Elliott and co-workers[95] examined a rigidly linked Ru(II)/Fe(II) complex in fluid solutions, and concluded that energy transfer proceeded by means of a through-space Dexter mechanism with an attenuation parameter of 2.0 Å^{-1}. Ohno and co-workers[96] investigated energy transfer in $Ru(bpy)_3^{2+}$ crystals doped with $Os(bpy)_3^{2+}$, and in that system, they estimate the attenuation parameter to be about 1.2 Å^{-1}, although even they remark that this value is somewhat low compared to the typically observed values. If we use these systems as a guidepost, they suggest that β should fall in the neighborhood of 1.2−2.1 Å^{-1}.

Table 1. Monte Carlo simulation parameters (k_0^{Ru} and k_0^{Os}) that yield best agreement between experiment and simulation for different values of the attenuation parameter, β and the most probable Ru*→Ru and Ru*→Os energy transfer times that are obtained from distributions like those shown in Figure 11

β (Å^{-1})	k_0^{Ru} (ns^{-1})	k_0^{Os} (ns^{-1})	τ_{max}^{Ru}	τ_{max}^{Os}
1.2	0.370	2.86	4.0	0.63
1.3	0.588	3.33	2.5	0.50
1.5	0.800	4.00	1.6	0.40
1.7	1.250	5.00	1.0	0.32
1.9	2.220	5.00	0.6	0.32

One limitation of this model is that the same polymer structure is used throughout the entire migration trajectory. This is clearly not the case in the experiment, especially for trajectories that span hundreds of nanoseconds. It is possible that the relative motion between complexes may facilitate energy migration, and by performing simulations on a "frozen" structure, this aspect of the dynamics is omitted. At the moment it is not clear how large this effect will be. Because of the dense loading, the space between the peripheries of the complexes is relatively small and thus large changes in the separation between nearest neighbors is probably not occurring to a great extent. What might be taking place, on the other hand, is that the identity of the nearest neighbors may be changing with time. Although each complex has 4−5 nearest neighbors, because of the exponential fall off in the rate constant with separation, only 1−3 of these are "connected" to the excited state through energy transfer. As the complexes move relative to each other some of these connections will be broken and new ones will be formed. The role that this plays in the energy migration process is currently under investigation and will be presented in a forthcoming publication.

3. Simulation Results. Since we cannot identify a unique value for the attenuation parameter, we have performed simulations for a range of β values between 1.2 and 2.1 Å^{-1}. The specific values investigated are listed in Table 1.

The simulation generates two emission transients: one for the Os growth and one for the Ru decay. These two transients were fit to the experimental data. For a given β, this was accomplished by adjusting only k_0^{Ru} and k_0^{Os}. The Ru transient was compared directly with the time-resolved emission detected at 640 nm, and the Os transient was compared to the emission detected at 780 nm, with the Ru contribution removed (Section C-1). The "goodness of fit" was determined by eye with special emphasis placed on the rise and rollover part of the transient (first 50−100 ns), the rational being that the majority of

(89) Gillespie, D. T. *J. Phys. Chem.* **1977**, *81* (25), 2340−2361.
(90) Hisada, K.; Ito, S.; Yamamoto, M. *J. Phys. Chem. B* **1997**, *101*, 6827−6833.
(91) Katayama, H.; Ito, S.; Yamamoto, M. *J. Phys. Chem.* **1992**, *96*, 10115.
(92) Katayama, H.; Maruyama, S.; Ito, S.; Tsujii, Y.; Tsuchida, A.; Yamamoto, M. *J. Phys. Chem.* **1991**, *95*, 3480.
(93) Kobashi, H.; Morita, T.; Mataga, N. *Chem. Phys. Lett.* **1973**, *20*, 376.
(94) Strambini, G. B.; Galley, W. C. *J. Chem. Phys.* **1975**, *63*, 3467.
(95) Larson, S. L.; Hendrickson, S. M.; Ferrere, S.; Derr, D. L.; Elliott, C. M. *J. Am. Chem. Soc.* **1997**, *119*, 9937. The value for the attenuation parameter, β, should be multiplied by 2.302.
(96) Tsushima, M.; Ikeda, N.; Nozaki, K.; Ohno, T. *J. Phys. Chem. A* **2000**, *104*, 5176.

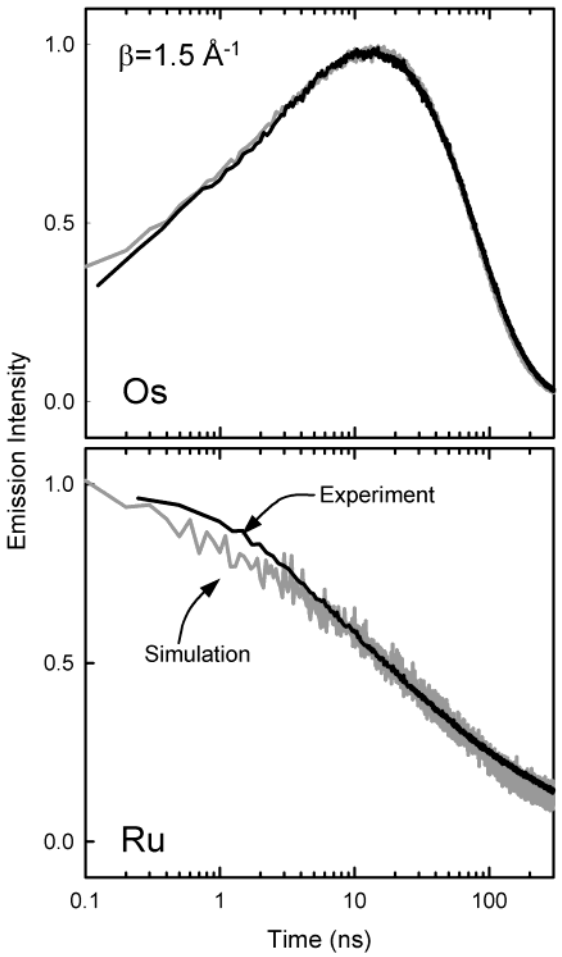

Figure 10. Comparison between the experimental data and the emission transients calculated by the simulation. The experimental Os transient corresponds to the emission detected at 780 nm minus the contribution from the Ru emission at that wavelength. The Ru transient is the emission detected at 640 nm.

sensitization events are occurring in this time window and should be weighted accordingly.

A comparison of the simulation results (obtained with $\beta = 1.5$ Å^{-1}) with the experimental data is shown in Figure 10. The time axis is plotted on a log scale to better represent both the short and long time aspects of the data. In both the Ru and Os cases there is excellent qualitative agreement between the simulation-generated transients and the experimental data. Overall, the agreement obtained with the other β values listed in Table 1 is qualitatively similar to that shown in Figure 10. Thus, we are unable to eliminate any of the β values listed in the table based solely on the inability of the simulation to reproduce the experimental data. This is not universally true, however, as there are some values of the attenuation parameter that do not reproduce the experimental data. We also examined β values outside this range and found that in general the quality of the fit deteriorates when β is less than 1.0 Å^{-1} or greater than 2.1 Å^{-1}. Reasonable agreement can be achieved with $\beta = 2.1$ Å^{-1}; however, the results are physically unreasonable ($k_0^{Ru} > k_0^{Os}$), and for this reason this value is omitted from the table.

The kinetics of the energy migration process are largely determined by the energy transfer rate constants that connect the metal centers. The distribution of the Ru*→Ru and Ru*→Os energy transfer rate constants is displayed in Figure 11, for the case where $\beta = 1.5$ Å^{-1}. Both distributions are highly asymmetric, with the larger rate constants (faster hopping times)

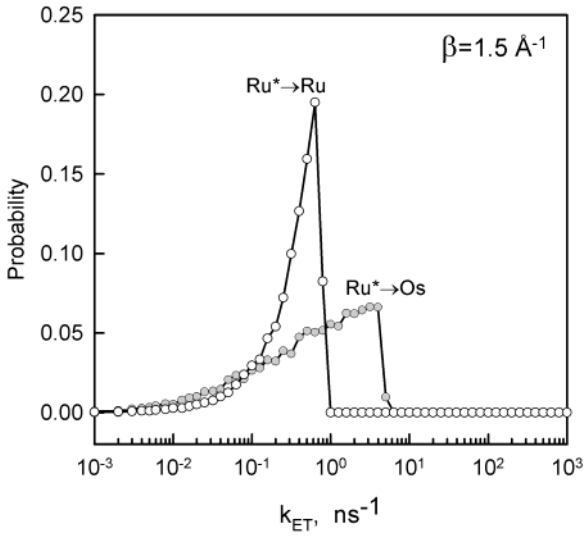

Figure 11. Distribution of rate constants for Ru*→Ru and Ru*→Os energy transfer observed during the Monte Carlo simulation.

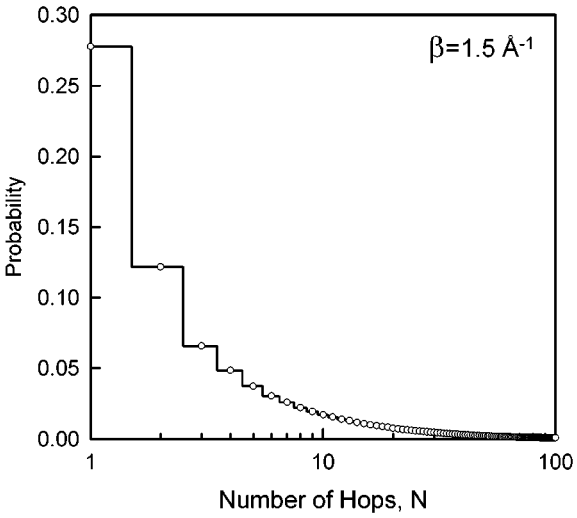

Figure 12. Distribution in the number of energy transfer jumps observed during a given trajectory. $N = 1$ corresponds to a single Ru*→Os step. $N > 1$ corresponds to $(N - 1)$ Ru*→Ru migration steps followed by one Ru*→Os step.

occurring more often. For the distributions shown in Figure 11, the most probable hopping times—denoted by τ_{max}^{Ru} and τ_{max}^{Os}—are 1.6 and 0.4 ns, respectively. It is interesting to note that the most probable Ru*→Os hopping time is similar in magnitude to the fast (400 ps) component observed in the rise of the sensitized Os emission (Section C-1), supporting the assignment that the fast kinetic component is due to Os sensitization by Ru excited states that are formed directly adjacent to Os traps. Displayed in Table 1 are the most probable hopping times observed for each β. The Ru*→Os energy transfer times are fairly insensitive to the value used for the attenuation parameter. This is not the case for the Ru*→Ru rate constant distribution, which shows a decrease in the hopping time with increasing β. The explanation for this trend is fairly simple.

As β is increased, the average distance that an excited Ru state can transfer on any given step is reduced. Hence, there is a definite correlation between β and the average number of hops an excited state takes before sensitization. The distribution of the number of Ru*→Ru hops that take place prior to sensitization is shown in Figure 12. Only migration trajectories that terminate in the sensitization of an Os site are included in this

distribution. The most probable number of hops occurs at $N = 1$, which corresponds to trajectories comprised of only the Ru*→Os energy transfer step. Although this prompt sensitization process is the most probable, it does not imply that Ru*→Ru energy migration is a minor component. Quite the contrary, the distribution has a long tail that extends to large *N*, indicating that there are some trajectories in which the excited state undergoes as many as 100 to 1000 Ru*→Ru steps. When these are added together they account for about 80% of the total probability, and thus the majority of trajectories involve some degree of Ru*→Ru migration. When the attenuation parameter is increased, the distribution in the number of Ru*→Ru hops shifts toward larger *N*, reflecting the smaller average distance per step.

A convenient measure of the polymer's performance is the efficiency of a single Ru*→Ru step, which can be defined in terms of the average hopping time as,

$$\chi_{ss} = 1 - \frac{\langle \tau_{Ru} \rangle}{\tau_{em}^{Ru}} \tag{9}$$

The single step efficiency associated with a Ru*→Ru hopping time on the order of 1−4 ns is in the range of 99.6−99.9%, suggesting that these polymeric systems could conduct excited-state energy over long distances without a significant loss in excited-state population. With a 99.6% single-step efficiency, an excited state could make 100 energy transfer jumps with an excited-state survival probability of about 65%. This increases to 90% when χ_{SS} is 99.9%.

IV. Summary and Implications

In this paper we present a detailed dynamics study of the excited state energy migration that occurs following photoexcitation of a multicentered assembly based on polypyridyl Ru(II) and Os(II) complexes. These results demonstrate that the Ru(II) derivatized polymers act as efficient "antennas" for collecting visible light and transferring its energy along the polymer backbone. This polymer system offers the design flexibility to readily create longer arrays, end functionalized arrays that have a single trap or charge-separating structure placed at one end, or nonrandom systems based on block copolymer architectures, all of which are currently under investigation in our laboratory. In addition to being soluble in a variety of nitrile solvents, it can also be embedded into plastic resins and inorganic glasses. This combined with its broad absorption throughout the visible makes it a candidate for use in molecular scale devices and solar energy conversion applications.

One path to optimizing the efficiency of these systems involves increasing the rate of Ru*→Ru self-exchange, for this will be the limiting factor in the overall efficiency of the polymer. It is possible that the chemical structure of the Ru(II) monomer units may play a role in the energy transfer rate. By replacing the *dab* ligands with *bpy* we can force the MLCT excitation to localize on the *mab* ligand rather than *dab*. We are beginning to investigate the role that the chemical structure of the monomer unit plays in the energy transfer process.

Another route to enhancing efficiency is extending the excited-state lifetime of the Ru(II) monomer units. This can be accomplished by ligand modification or by immersing the polymer into rigid solvents. The use of rigid environments can increase the Ru lifetime by a factor of 2 or more. Thus, to the extent that the energy transfer times remain the same, the increase in lifetime afforded by the rigid solvent could greatly enhance the overall efficiency of the molecular assemblies. Presently we are investigating the energy transfer dynamics of these molecular arrays doped into polymer films and silica xerogel monoliths. These room temperature rigid solvents are attractive in terms of their ease of proccessing and long-term stability needed for potential molecular device applications.

Acknowledgment. Funding for this project was provided by the U.S. Department of Energy (DE-FG02-96ER14607) and the Research Corporation (RI0048). We thank Dr. Dan Allen Myers from Kinston, North Carolina, whose gift to the UNC-CH Faculty Partners Fund also provided support for this project.

Appendix

The stochastic kinetic algorithm is adapted from Gillespie.[89] The calculation requires the selection of two random numbers, r_1 and r_2, from a uniform distribution on the interval (0,1). One of the random numbers is used to calculate the amount of time it will take the step to occur, i.e.

$$\Delta t = \frac{1}{\sum k} \ln\left(\frac{1}{r_1}\right) \tag{10}$$

where $\sum k$ is the sum of all rate constants for all the pathways (energy transfer and deactivation) leading from the initial excited state; i.e., $\sum k = (k_{i,1} + k_{i,2} + k_{i,3} \cdots k_{i,20} + k_{em})$, where $k_{i,1}$ is the rate constant for energy transfer from *site i* to *site 1*. The second random number is used to determine which of the possible pathways (e.g. energy transfer to another site, excited-state decay, etc.) the system will follow. The probability that the excited state will transfer to *site 1*, for example, is given by

$$P_{i,1} = \frac{k_{i,1}}{\sum k} \tag{11}$$

The selection of the pathway is then fairly straightforward. The interval (0,1) is divided into 20 subintervals, the sizes of which are given by the probabilities for each of the 19 possible energy transfer pathways and excited-state deactivation. The interval in which the second random number, r_2, lies corresponds to the pathway that the system follows. After selecting the pathway, the simulation time is increased by Δt, i.e. $t = t + \Delta t$, and a new step is initiated.

JA016304I